analytical chemistry

pubs.acs.org/ac
Article

Ion Mobility Gas-Phase Separation Enhances Top-Down Mass Spectrometry of Heavily Modified Guide RNA

Luis A. Macias, Jamie Lowther, Eric L. Tillotson, Ellen Rohde, and James A. Madsen*

Cite This: *Anal. Chem.* 2025, 97, 9430−9437
Read Online

ACCESS | Metrics & More | Article Recommendations | Supporting Information

ABSTRACT: As gene editing technologies enter the clinic, state-of-the-art characterization methods have been developed in parallel to assess the components of these paradigm-shifting medicines. One such component, the guide RNA (gRNA) element of CRISPR-based drugs, is a large synthetic heavily modified oligonucleotide that programs for the desired gene edit. Conventional oligonucleotide sequencing technologies can inform gRNA composition, but these methods may not completely capture the chemical modifications that are introduced during synthesis. Circumventing these challenges, mass spectrometry has demonstrated use in oligonucleotide analyses and has been combined here with ion mobility to deepen its characterization power. The use of ion mobility enabled us to perform gas-phase separation of the fragment ions produced by top-down mass spectrometry, yielding a significant increase in fragment identifications for a highly modified 100-mer gRNA by uncovering high-confidence assignments for heavily modified regions and for the important spacer region. Furthermore, the high-confidence fragment assignments empowered simultaneous *de novo* sequencing and chemical modification localization for the 5′-end spacer region as well as for 15 nucleotides on the heavily modified 3′-end. Overall, a total sequence coverage of 95% was achieved for the heavily modified 100-mer, ushering near complete sequence and chemical modification confirmation by top-down mass spectrometry.

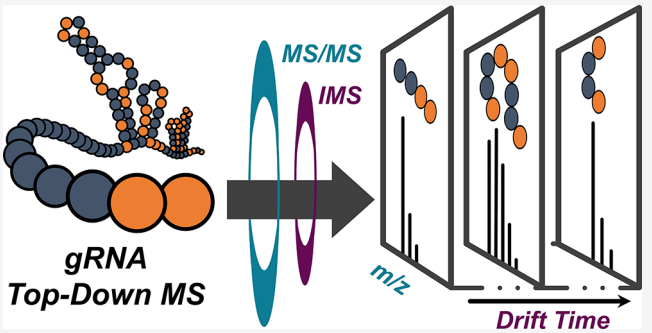

INTRODUCTION

Within the past decade, meteoric breakthroughs have propelled CRISPR-based gene editing therapies as disease-modifying and potentially even curative treatments for genetic diseases. Representative applications of this technology currently comprise *in vivo* and *ex vivo* therapies to address cardiovascular,[1−3] autoimmune,[4] neurodegenerative,[5,6] and rare diseases,[7] including an *ex vivo* treatment for sickle cell disease that matured into the first approved CRISPR-based therapy.[8] Key components of such drugs are the guide RNA (gRNA) and the gene editing enzyme,[7,9−11] as well as custom drug delivery vehicles tailored to distinct modalities or targets.[3,7,10,12,13] In all cases, drug activity depends on the formation of a ribonucleoprotein (RNP) complex between the tracr region of the gRNA and a gene editing enzyme, enabling the gRNA spacer sequence to lead the genome modifying RNP to the desired edit site.[7,9,10] Moreover, because the gRNA sequence is the main determinant of the induced edit site, robust characterization of gRNA chemistry is commensurate with drug efficacy.

gRNA for CRISPR-based drugs is commonly generated by chemical synthesis to a length of ∼100 nucleotides and often incorporates chemical modifications on the sugar moieties or phosphate backbone to increase gRNA stability and efficiency.[14] The first ∼20 nucleotides on the 5′-end constitute the spacer region, specifying the desired gene edit site, while the remainder of the sequence comprises the tracr region, which complexes with the gene editing enzyme to form a functional RNP.[14] Because errors may occur during chemical synthesis, ascertaining high sequence fidelity, particularly in the spacer region, is linked to accurate and efficient editing. Conventional oligonucleotide sequencing technologies, such as next-generation sequencing (NGS)[15] or PacBio,[16] can be employed for gRNA analysis. However, these indirect strategies require reverse transcription of RNA into DNA prior to sequencing, leading to the loss of chemical modifications and nonquantitative assessments of sequence impurities.[16−19] These drawbacks hinder characterization of gRNA but may be supplemented by the use of orthogonal technologies that directly interrogate the gRNA structures. Oxford Nanopore sequencing, for example, is capable of detecting some chemical modifications but requires the use of challenging or uncommon base calling routines.[16,20]

Received: February 1, 2025
Revised: March 25, 2025
Accepted: April 1, 2025
Published: April 11, 2025

https://doi.org/10.1021/acs.analchem.5c00705
Anal. Chem. 2025, 97, 9430−9437

Notably, mass spectrometry (MS) based strategies have proved highly effective for biomolecular characterization assays, including oligonucleotide sequencing.[21−31] Both bottom-up strategies,[32−42] where oligonucleotides are digested into smaller fragments prior to MS analysis, and top-down strategies,[19,26,30,43−49] entailing direct sequencing of the intact oligonucleotides, have been successfully used to characterize gRNA.[19,32−34,43] In either modality, tandem mass spectrometry (MS/MS) is applied to fragment the oligonucleotide backbone, generating fragment ions that inform the nucleotide sequence as well as the presence of chemical modifications.[50,51] Furthermore, we have previously demonstrated that the rich and complex fragment spectra produced in top-down analyses of heavily modified gRNA can be mined to identify and quantify potential impurities.[19] Here, we amplify both the number of fragment ions assigned and the confidence in each assignment by implementing ion-mobility gas-phase separation of product ions to thoroughly interrogate the dense top-down spectra that are generated from highly modified gRNA.

EXPERIMENTAL SECTION

Materials. LCMS grade water, methanol, acetonitrile, and formic acid were acquired from Fisher Scientific (Hampton, NH). LCMS grade triethylamine (TEA) and hexafluoroisopropanol (HFIP) were purchased from CovaChem (Loves Park, IL) and Millipore Sigma (St. Louis, MO), respectively.

All gRNA samples were procured from Integrated DNA Technologies (IDT; Coralville, IA), and were purified to enrich for the full-length product by anion exchange chromatography. Prior to analysis, samples were concentrated to 10 mg/mL using 10k MWCO filters. The gRNA sequence is shown in Table S1.

Liquid Chromatography. Chromatographic separations were performed on a Waters Acquity UPLC H-Class Plus system (Milford, MA) using a XBridge, C18, 5 μm, 4.6 mm × 50 mm column temperature controlled at 30 °C. Mobile phase A (MPA) was composed of 100 mM HFIP, 16.3 mM TEA, and 1% methanol. Mobile phase B (MPB) was a mixture of 50/50 methanol and acetonitrile. Mobile phase C comprised of 50% methanol and 0.1% formic acid. Chromatography was performed at a constant flow rate of 250 μL/min, starting at 95% MPA and 5% MPB, and a linear ramp to 85% MPA and 15% MPB over 21 min, followed by 100% MPC, before returning to 95% MPA and 5% MPB for equilibration. Injections were performed with 20 μL of sample.

Mass Spectrometry and Ion Mobility. All data were collected on the Waters SELECT series cyclic ion mobility spectrometry (IMS) mass spectrometry system coupled to the liquid chromatography (LC) system by electrospray ionization (ESI) in the negative ion mode. MS/MS was performed in W-mode with a transfer CE of 37 V, and a wide isolation window centered at 1226 m/z. For ion mobility, traveling wave (TW) static height was set to 19 V with cyclic and array TW velocity set to 375 m/s. Spectra rate was set to 1 Hz. Instrument source conditions were set to 1.5 kV capillary voltage, 45 V cone voltage, 10 V source offset, 550 °C desolvation temp, 800 L/h desolvation gas, and 6.0 bar nebulizer gas. To apply a wide isolation window, quadrupole LM resolution (low) and LM resolution (high) were both set to 0.0. Collision gas 1 was set to 3.5 mL/min. RF settings were set to 250 stepwave RF, 700 ion guide RF, 400 trap RF, 300 drift cell RF, 350 pre/post RF, and 250 cyclic RF. The IMS sequence comprised three steps: (1) inject, (2) separate, and (3) eject and acquire. Prearray gradient, prearray bias, postarray gradient, and postarray bias were set to 85, 70, 35, and 10 V, respectively, for each step in the cIMS sequence. Array entrance, array TW height, array offset, and array exit were set as 10 V, 2 V, 45 V, and 50 V for the inject step, as 30 V, 0, 70 V, and 30 V for the separate step, and set as 50 V, 25 V, 45 V, and 2 V for the eject and acquire step.

Data Analysis. Raw data files were imported into DriftScope to select all spectra collected during elution of the full-length product and then exported as a raw file to retain drift time but no retention time dimension. The raw files were then converted into mzml format, followed by custom analyses performed with python. Further information regarding fragment assignment, spectrum recalibration, FDR estimates, and *de novo* sequencing are included in the Supporting Information.

RESULTS AND DISCUSSION

To develop this gRNA characterization strategy, an appropriate ion mobility spectrometry (IMS) enabled MS platform was selected. IMS achieves separation by applying an electric field to push ions through a buffer gas, resulting in differing electrophoretic mobilities based on ion size, shape and charge.[52−54] Multiple versions of IMS-MS platforms are available, each featuring unique advantages or drawbacks suited for disparate applications.[52−54] Recently, the cyclic IMS-MS system (cIMS)[55] has demonstrated utility in the decongestion of protein top-down spectra,[56] presenting a promising platform apt for enhancing intact gRNA analyses. Utilizing this platform, an MS/MS-IMS gas phase separation workflow was devised as illustrated in Scheme 1 and detailed in the Supporting Information. Briefly, intact gRNAs are introduced into the instrument via liquid chromatography electrospray ionization (LC-ESI) in the negative ion mode, followed by quadrupole isolation of low charge state precursor ions using a wide (∼150 m/z) isolation window. A chromatogram and intact MS1 spectrum for gRNA X are shown in Figure S1. Low charge state precursor ions were selected to promote production of sequence ions over less informative fragmentation pathways, including neutral losses, base losses, and internal fragmentation, which are favored when dissociating precursors with a higher charge density.[57,58] The gRNA ions are then collision activated to induce backbone bond cleavages throughout the sequence (Scheme 2) and generate a mixture of fragment ions, predominantly c- and y-type, that are then separated by a single pass through the cIMS cell. This process yields a series of spectra, where each spectrum is associated with a specific drift time, that can then be individually searched through to identify gRNA sequence fragments. Importantly, this workflow results in a reduced number of fragment ions per spectrum, facilitating confident assignment.

Advantages of IMS are evident in comparisons of top-down spectra collected for intact gRNA with and without implementing gas-phase separation. Figure 1 shows narrow m/z windows of the MS/MS spectra collected for top-down analyses targeting the 25-, 26-, and 27- charge states (in a single acquisition using a wide isolation window of ∼150 m/z) of the 100-mer gRNA X (sequence shown in Table S1) both with and without the IMS capabilities of the cIMS instrument; the window shown in Figure 1A focuses on m/z 1239−1242 which appears congested when IMS is not employed, precluding assignment of any sequence ions within this region

https://doi.org/10.1021/acs.analchem.5c00705
Anal. Chem. 2025, 97, 9430−9437

Scheme 1. Summary of LC-MS/MS-IMS Strategy[a]

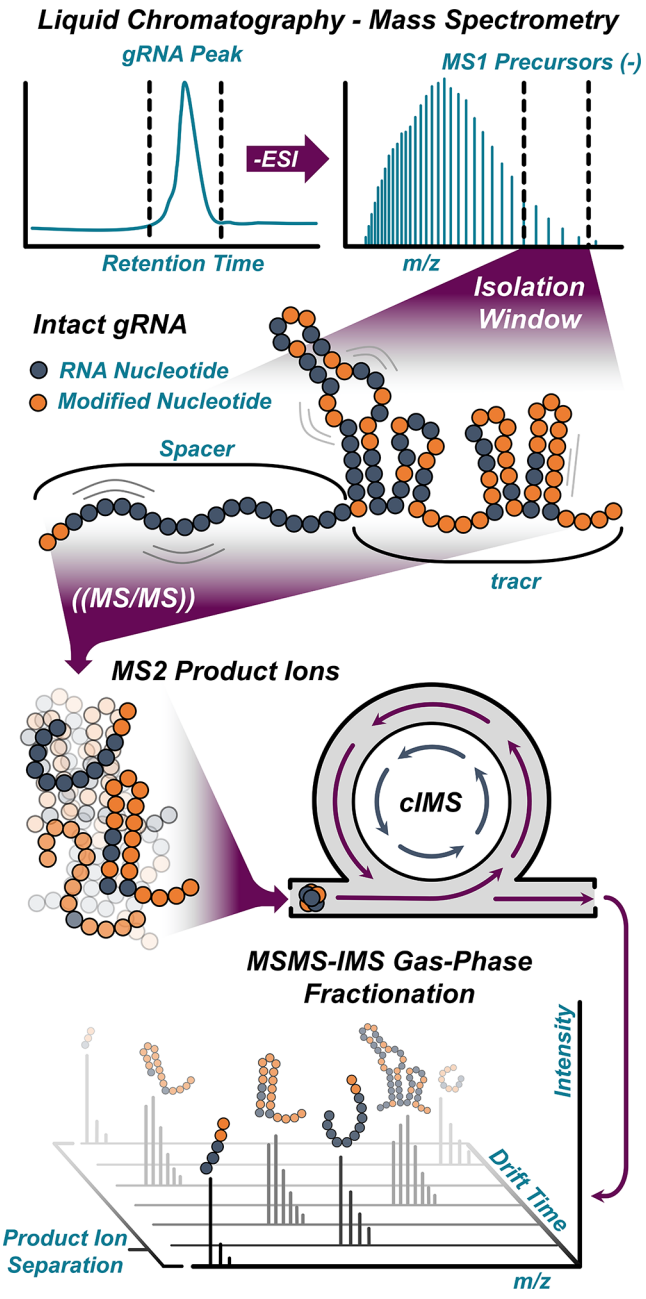

[a]Intact gRNA is introduced into the MS via LC-ESI in the negative ion mode. Low charge state precursors are quadrupole isolated with a wide m/z window and subjected to collisional activation. The resulting ion cloud, including a mixture of product ions, is separated with the cIMS system to produce a set of spectra, where each spectrum is associated with a unique drift time value.

Scheme 2. Possible Backbone Cleavages and Associated Fragment Type Generated during Oligonucleotide MS/MS[a]

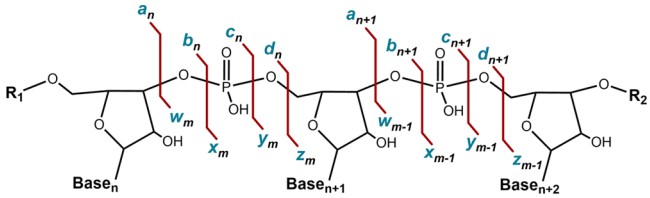

[a]Nucleotide position from the 5′-end is denoted by n, while m denotes the length of the oligonucleotide minus n.

(full MS/MS spectrum is shown in Figure S2A). In contrast, utilizing IMS uncovers previously hidden fragment ions c_{19}^{5-} and c_{64}^{17-} (Figure 1B,C) at 23.0 and 33.1 ms of drift time, respectively, highlighting the ability of MS/MS-IMS to garner elusive details from top-down analyses (3D view of MS/MS-IMS data is show in Figure S2B). Similarly, Figure 1D shows an instance of two fragment ions sharing m/z space in a typical MS/MS experiment collected without IMS. In this example, isotopic envelopes for two distinct fragment ions overlap and distort one another, obfuscating identification. Again, IMS allows these fragment ions to be resolved in the drift time dimension, enabling assignment of y_{12}^{4-} and y_9^{3-} at 23.4 and 25.2 ms of drift time, respectively (Figure 1E,F). Additional examples of fragment ions observed by MS/MS-IMS but not by MS/MS are displayed in Figure S3. As exemplified across these comparative spectra, fragment ions present at congested spectral regions (usually adjacent to precursor ions), large fragment ions with low signal (such as c_{64}) and sets of fragment ions with overlapping m/z values challenge fragment assignment, yet gas-phase separation ameliorates these issues to empower confident identification of otherwise intractable product ions.

To fully capitalize on the highly informative MS/MS-IMS data, an automated data analysis workflow was created to mine the spectra for sequence fragments. This workflow is based on previously reported custom analyses[19] and is further detailed in the Supporting Information. First, to ensure robust and adequate performance of the data analysis, m/z values were recalibrated to minimize mass drift that occurred during MS/MS-IMS experiments on this platform and maintain the mass error window within ±5 ppm (Figure S4). Additionally, cosine similarity scores were used to ascertain high isotopic fidelity by measuring similarity between theoretical and observed isotopic distributions of potential fragment assignments. Using these scores, a cosine score threshold was determined by estimating false discovery rate (FDR) via a target-decoy approach, using a previously described method,[19,59,60] and selecting a score threshold that approximated a 1% FDR. Cosine similarity score distributions measured for decoy and target spectra are shown in purple and orange, respectively, for MS/MS and MS/MS-IMS of gRNA X in Figure 2A,B. In both experiment types, the target distribution appeared to be bimodal, where one broader distribution, centered near a cosine score of ∼0.6, aligns with the observed decoy distribution and likely arises from false assignments, while the secondary distribution observed at higher cosine scores (>0.9) likely corresponds to true positives. Notably, the separation between the two distributions is significantly more obvious in the MS/MS-IMS data, suggesting that ion mobility separation improves classification of false and true assignments by promoting higher isotopic fidelity.

Realizing the advantages of IMS gas-phase separation combined with automated analysis, a search for only c- and y-type fragment ions with a 1% FDR revealed a substantial improvement in characterization power for the MS/MS-IMS workflow over a typical MS/MS experiment. Limiting the search to c- and y-type fragment ions constrained the search space to the most abundant fragment ions generated via collisional activation of RNA, maximizing sequence coverage while curtailing spurious identifications to less common fragment types. Figure 2C and Figure 2D summarize the

https://doi.org/10.1021/acs.analchem.5c00705
Anal. Chem. 2025, 97, 9430−9437

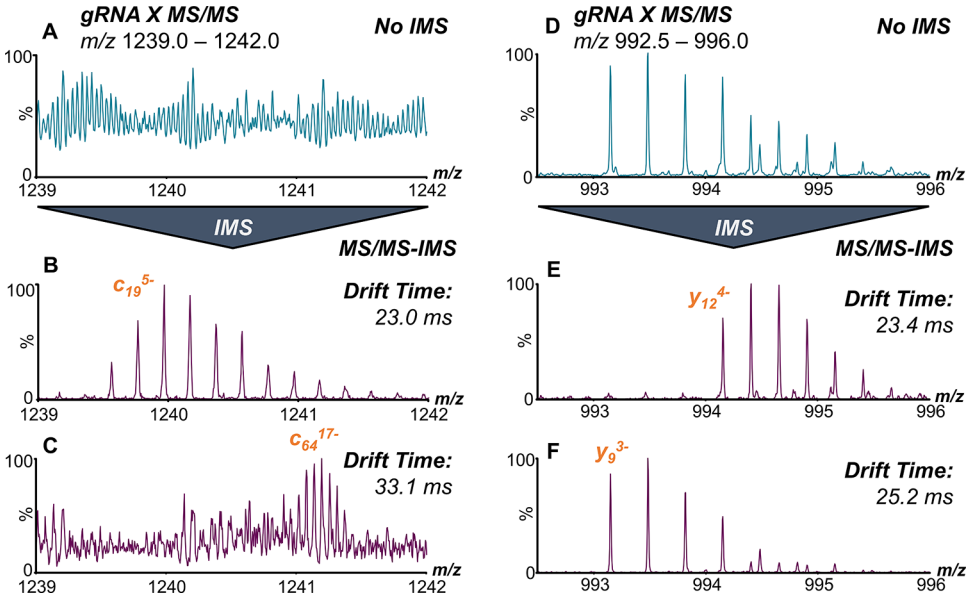

Figure 1. Examples of gRNA product ions resolved by IMS. Mass window showing m/z 1239.0−1242.0 in the MS/MS experiment (A) compared to the same mass window in the MS/MS-IMS experiment at 23.0 ms (B) and 33.1 ms (C) of drift time where fragments c_{19}^{5-} and c_{64}^{17-} can be identified, respectively. Mass window showing m/z 992.5−996.0 in the MS/MS experiment (D) compared to the same mass window in the MS/MS-IMS experiment at 23.4 ms (E) and 25.2 ms (F) of drift time where fragments y_{12}^{4-} and y_9^{3-} can be identified, respectively.

fragment identifications (listed in Tables S2 and S3) produced from gRNA X with a cosine score of >0.94, corresponding to an FDR of 1.1% in the MS/MS experiment and 1.0% in the MS/MS-IMS data. While the MS/MS data yielded a sequence coverage of 61%, the demonstrated increase in fragment assignments afforded by the MS/MS-IMS workflow increased total sequence coverage up to 95%, providing near complete coverage of the heavily modified gRNA. Because both strategies provide complete coverage of the spacer sequence, the observed gains in coverage arise from fragment ions mapped to the tracr region, a stretch of nucleotides predominantly populated by 2′-O methylations. These modifications are known to provide resistance to backbone cleavage during collisional activation,[61] suppressing coverage of the tracr in typical MS/MS analyses which may be rescued by leveraging gas-phase separation as evidenced here. Furthermore, even if the cosine score cutoff is set to an extremely stringent >0.98 cosine score threshold (approximating 0.1% FDR), a sequence coverage of 78% is still achieved while maintaining full coverage of the spacer sequence in the MS/MS-IMS spectra (Figure S5B); in contrast, the MS/MS experiment with no IMS only achieves a 41% coverage and fails to fully sequence the spacer (Figure S5A), highlighting the notable increase in isotopic fidelity uncovered by IMS separation. Overall, gas-phase separation unequivocally imparts deeper characterization, as witnessed in these contrasting cleavage maps.

Moreover, the increased accuracy in fragment assignment also translates into improved *de novo* sequencing. Although conventional oligonucleotide sequencing by NGS and PacBio can deduce the base sequence of large synthetic nucleotides by *de novo* means, these methods cannot characterize the sugar moiety and phosphate linker, a drawback that does not necessarily apply to MS/MS based strategies. We previously reported *de novo* characterization of the gRNA 5′-end via MS/MS;[19] however, the strategy required decoupling the *de novo* assignment of the nucleotide base sequence from *de novo* assignment of chemical modifications such that either the base sequence or modification positions had to be provided for the strategy to be successful. Because improvements in fragment assignment reduced false assignments and thus the overall search space while constructing MS/MS *de novo* sequences, this limitation did not impact MS/MS-IMS *de novo* gRNA sequencing, as demonstrated for gRNA X (Tables S4 and S5). In this iteration, each nucleotide position n can be assigned to one of the 12 nucleotides (rA, rG, rC, rU, mA, mG, mC, mU, mA*, mG*, mC*, mU*) that comprise this sequence while providing no other knowledge. Using this method to sequence the 5′-end, the top *de novo* candidate perfectly aligned with all 20 nucleotides of the spacer region, matching both the base sequence and the positions of the chemical modifications (Table S4). Although three other lower-scoring sequence candidates were identified, these were speculated to occur due to potential n-1 and n-2 truncations confounding fragment assignment; the presence of these impurities was then confirmed by conducting a sequence search for both species and detecting several *c*-type ions on the 5′-end that are unique to the truncated species (Figure 3A and Figure 3B, with identified fragments listed in Tables S6 and S7, respectively).

Similarly, the top candidate identified by *de novo* sequencing of the first 15 nucleotides on the 3′-end was also an exact match to the heavily modified nucleotide sequence of gRNA X (Table S5). Other lower scoring candidates included G to A* substitutions, G to A substitutions, or combinations thereof. Due to the similar mass differences between G/A and PS/PO conversions (±15.995 Da and ±15.977) translating into even smaller m/z differences at higher charge states, the G to A* substitutions (featuring a difference of 0.0045 m/z in the 4- charge state) are explained as misassignments due to the theoretical +A* m/z being within the ±5 ppm error window of the actual +G nucleotide. Likewise, the G to A substitutions were rationalized to originate from a potential PS to PO impurity on the 3′-end, as this would result in a similar misassignment. To confirm the presence of the PS to PO

https://doi.org/10.1021/acs.analchem.5c00705
Anal. Chem. 2025, 97, 9430−9437

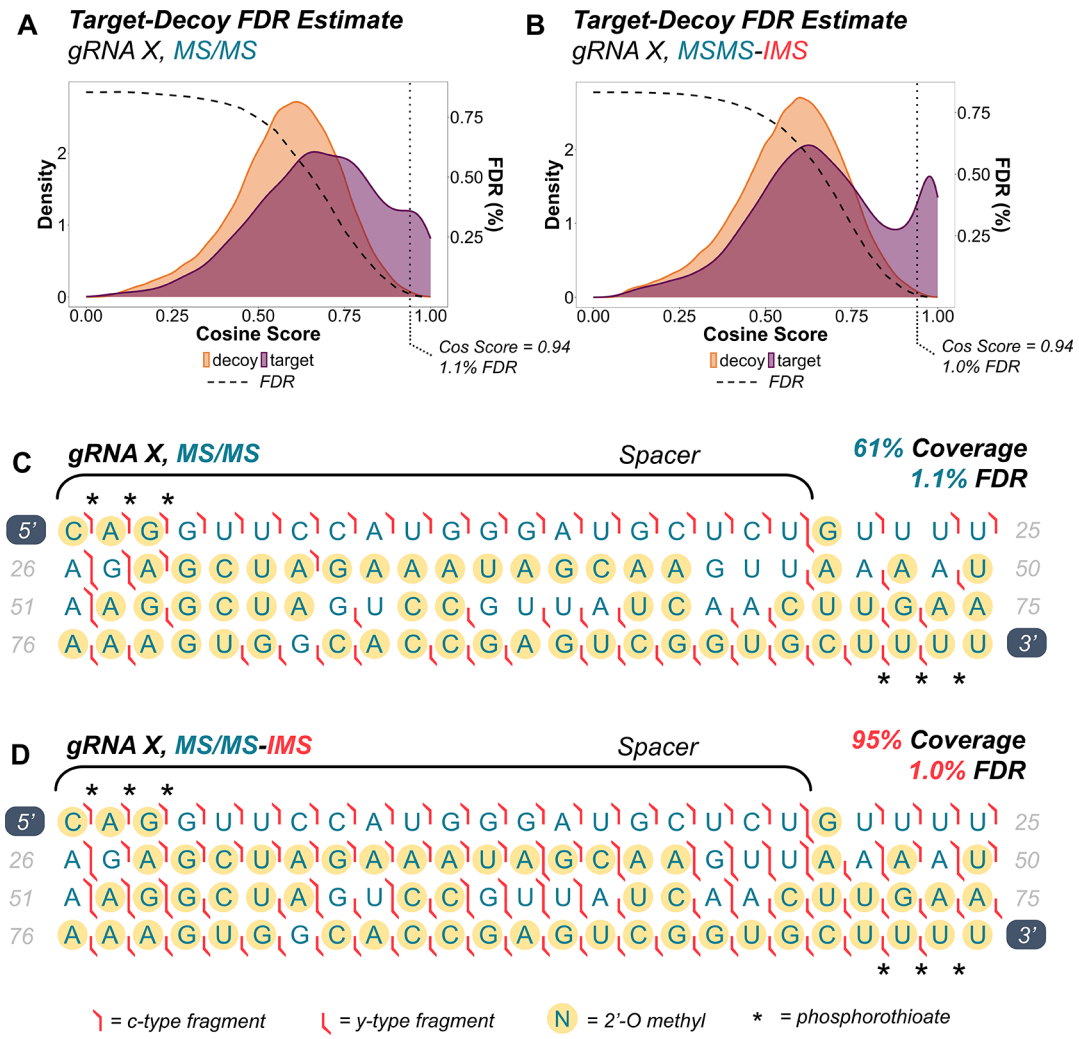

Figure 2. Comparison of target-decoy cosine score distributions for MS/MS (A) and MS/MS-IMS (B) top-down experiments for gRNA X. Cosine scores for decoy and target hits are represented by the orange and purple distributions, respectively. The black dashed line represents the FDR estimated at a given cosine score. The vertical dotted line marks the cosine score threshold closest to 1% FDR, corresponding to 0.94 in both experiments. Comparison of coverage maps produced by MS/MS (C) and MS/MS-IMS (D) of gRNA X, at a 1% FDR. A total coverage of 61% and 95% was achieved for the MS/MS and MS/MS-IMS experiment, respectively. Full coverage of the spacer was achieved in both cases.

impurity, fragment ions for a PS to PO conversion on the 3′-end were searched for and found throughout the 3′-end, as demonstrated in Figure 3C and Table S8, explaining the source of the incorrect G to A candidates. Even though complete sequencing is not yet possible, these results nonetheless show the power of *de novo* sequencing of gRNA 5′- and 3′-ends by MS/MS-IMS and its potential uses in informing gRNA chemistry.

CONCLUSIONS

Here, IMS gas-phase separation is employed to counter common complications encountered within top-down MS/MS spectra of highly modified gRNA. In short, mixtures of sequence ions produced upon collisional activation of large oligonucleotides are complex, yielding spectra with a wealth of fragment signals that often overlap and stunt fragment assignments. Consequently, distorted isotopic distributions and low intensity fragment ions compounded with high noise levels hamper data analysis in traditional MS/MS spectra. To remedy these issues, IMS was mended into the strategy post collisional activation to effectively separate the resultant mixture of product ions. MS/MS-IMS relieved spectral congestion and bolstered total fragment assignments by increasing isotopic fidelity. With MS/MS-IMS, near complete coverage of a heavily modified 100-mer gRNA was attained, exhibiting improved coverage even for regions of the oligonucleotide sequence marked by many 2′O-methylations, a chemical modification known to inhibit fragmentation. Although complete *de novo* sequencing was not achieved here, further developments in sensitivity and mass accuracy, as well as adapting additional advancements that stem from IMS, namely collisional cross section prediction and matching,[62] could lead to even more accurate and extensive oligonucleotide fragment identifications, and potentially resolve isobaric assignments (i.e., A*/G conversions) during *de novo* sequencing. All this information characterizing gRNA was garnered from a single LC-MS/MS-IMS acquisition using a 31 min method. While CRISPR-based and oligonucleotide therapeutics present novel constructs and chemistry aimed for the clinic, top-down mass spectrometry armed with ion mobility and other technologies could become the method of choice to sequence oligonucleotides, inform oligonucleotide

https://doi.org/10.1021/acs.analchem.5c00705
Anal. Chem. 2025, 97, 9430−9437

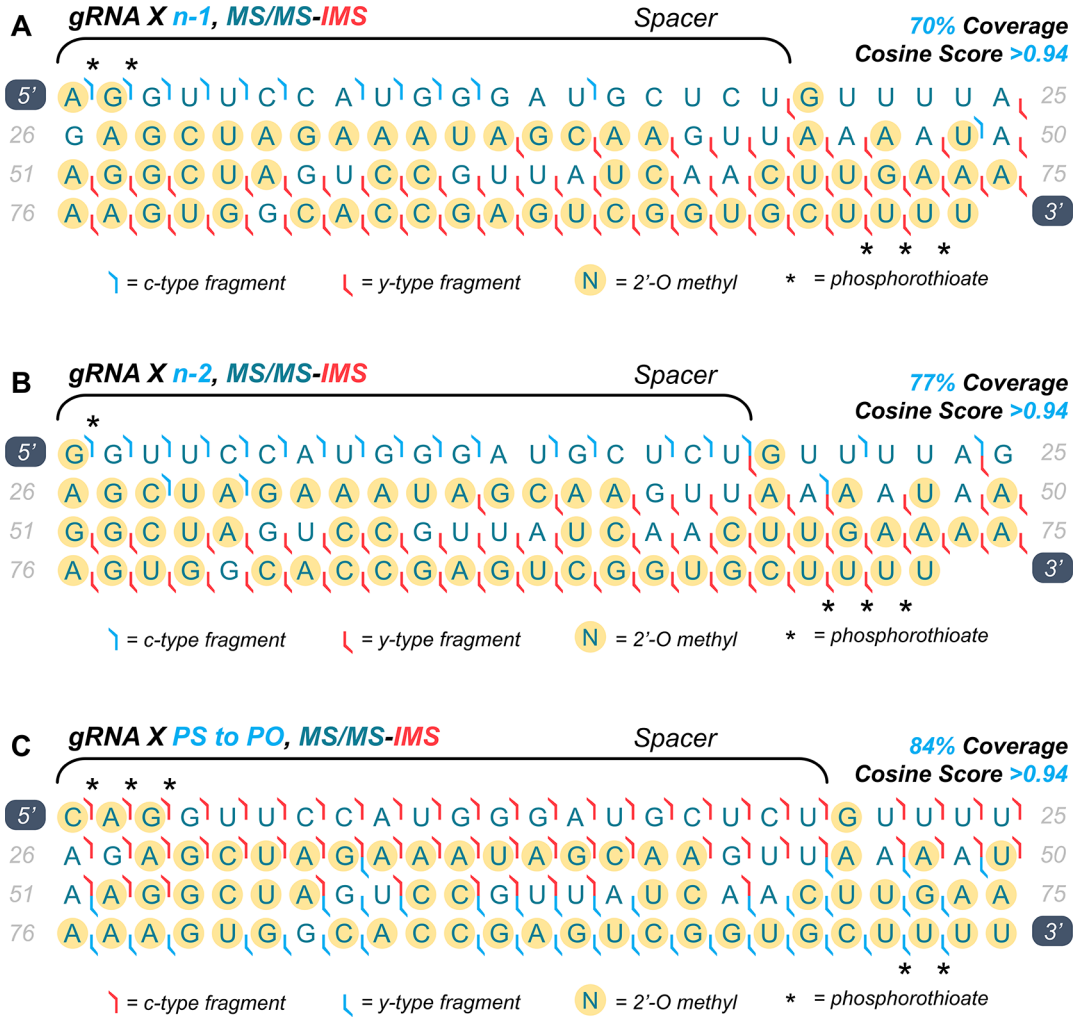

Figure 3. Coverage maps for potential impurities in gRNA X, including 5′-truncation n-1 (A), 5′-truncation n-2 (B), and PS to PO conversion on the 3′-end (C). Blue cleavage marks indicate identified fragment ions that are unique to the impurity, whereas cleavage marks in red are expected to be shared between the impurity and full-length product. Only fragments with a cosine score of >0.94 are shown, to align with the 1.0% FDR calculated in Figure 2.

synthetic chemistry, and characterize impurities in these prospective medicines.

■ ASSOCIATED CONTENT

Supporting Information

The Supporting Information is available free of charge at https://pubs.acs.org/doi/10.1021/acs.analchem.5c00705.

Additional experimental details, gRNA sequence, de novo results, sample spectra, chromatogram, supplemental coverage maps, and mass errors before and after recalibration (PDF)

Lists of fragment ions identified by MS/MS and MS/MS-IMS (XLSX)

■ AUTHOR INFORMATION

Corresponding Author

James A. Madsen − *Verve Therapeutics, Boston, Massachusetts 02215, United States;* orcid.org/0009-0009-2512-8944; Email: jmadsen@vervetx.com

Authors

Luis A. Macias − *Verve Therapeutics, Boston, Massachusetts 02215, United States;* orcid.org/0000-0003-1949-6029

Jamie Lowther − *Verve Therapeutics, Boston, Massachusetts 02215, United States*

Eric L. Tillotson − *Verve Therapeutics, Boston, Massachusetts 02215, United States*

Ellen Rohde − *Verve Therapeutics, Boston, Massachusetts 02215, United States*

Complete contact information is available at: https://pubs.acs.org/10.1021/acs.analchem.5c00705

Author Contributions

L.A.M., J.A.M., and E.R. conceived, designed, and directed the top-down gRNA MS/MS-IMS methodology. L.A.M. executed laboratory experiments and performed data analysis. L.A.M. and J.A.M. wrote the manuscript. J.L. and E.T. performed gRNA purification. E.R. supervised and provided oversight of the work. All authors reviewed and provided comments on the manuscript.

https://doi.org/10.1021/acs.analchem.5c00705
Anal. Chem. 2025, 97, 9430−9437

Notes

The authors declare the following competing financial interest(s): All authors are employees and own equity in Verve Therapeutics.

■ ACKNOWLEDGMENTS

This study was supported by funding from Verve Therapeutics.

■ REFERENCES

(1) Musunuru, K.; Chadwick, A. C.; Mizoguchi, T.; Garcia, S. P.; DeNizio, J. E.; Reiss, C. W.; Wang, K.; Iyer, S.; Dutta, C.; Clendaniel, V.; et al. *Nature* **2021**, *593* (7859), 429−434.
(2) Asif, M.; Khan, W. J.; Aslam, S.; Aslam, A.; Chowdhury, M. A. *Cureus* **2024**, *16* (4), No. e57869.
(3) Kasiewicz, L. N.; Biswas, S.; Beach, A.; Ren, H.; Dutta, C.; Mazzola, A. M.; Rohde, E.; Chadwick, A.; Cheng, C.; Garcia, S. P.; et al. *Nat. Commun.* **2023**, *14* (1), 2776.
(4) Lee, M. H.; Shin, J. I.; Yang, J. W.; Lee, K. H.; Cha, D. H.; Hong, J. B.; Park, Y.; Choi, E.; Tizaoui, K.; Koyanagi, A.; et al. *International Journal of Molecular Sciences* **2022**, *23* (3), 1337.
(5) Thapar, N.; Eid, M. A. F.; Raj, N.; Kantas, T.; Billing, H. S.; Sadhu, D. *Ann. Med. Surg.* **2024**, *86* (1), 329−335.
(6) Nouri Nojadeh, J.; Bildiren Eryılmaz, N. S.; Ergüder, B. İ. *EXCLI J.* **2023**, *22*, 567−582.
(7) Li, Q.; Gao, Y.; Wang, H. *Life* **2022**, *12* (12), 1968.
(8) Adashi, E. Y.; Gruppuso, P. A.; Cohen, I. G. *Am. J. Med.* **2024**, *137* (5), 390−392.
(9) Jinek, M.; Chylinski, K.; Fonfara, I.; Hauer, M.; Doudna, J. A.; Charpentier, E. *Science* **2012**, *337* (6096), 816−821.
(10) Li, T.; Yang, Y.; Qi, H.; Cui, W.; Zhang, L.; Fu, X.; He, X.; Liu, M.; Li, P.-f.; Yu, T. *Signal Transduction and Targeted Therapy* **2023**, *8* (1), 36.
(11) Jiang, F.; Doudna, J. A. *Annual Review of Biophysics* **2017**, *46* (46), 505−529.
(12) Nelson, C. E.; Gersbach, C. A. *Annu. Rev. Chem. Biomol. Eng.* **2016**, *7* (7), 637−662.
(13) Madigan, V.; Zhang, F.; Dahlman, J. E. *Nat. Rev. Drug Discovery* **2023**, *22* (11), 875−894.
(14) Allen, D.; Rosenberg, M.; Hendel, A. *Frontiers in Genome Editing* **2021**, *2*, Review.
(15) Goodwin, S.; McPherson, J. D.; McCombie, W. R. *Nat. Rev. Genet.* **2016**, *17* (6), 333−351.
(16) Hook, P. W.; Timp, W. *Nat. Rev. Genet.* **2023**, *24* (9), 627−641.
(17) Potapov, V.; Fu, X.; Dai, N.; Corrêa, I. R., Jr.; Tanner, N. A.; Ong, J. L. *Nucleic Acids Res.* **2018**, *46* (11), 5753−5763.
(18) Munafó, D. B.; Robb, G. B. *RNA* **2010**, *16* (12), 2537−2552.
(19) Macias, L. A.; Garcia, S. P.; Back, K. M.; Wu, Y.; Johnson, G. H.; Kathiresan, S.; Bellinger, A. M.; Rohde, E.; Freitas, M. A.; Madsen, J. A. *ACS Central Science* **2023**, *9* (7), 1437−1452.
(20) Wang, Y.; Zhao, Y.; Bollas, A.; Wang, Y.; Au, K. F. *Nat. Biotechnol.* **2021**, *39* (11), 1348−1365.
(21) Santos, I. C.; Lanzillotti, M.; Shilov, I.; Basanta-Sanchez, M.; Roushan, A.; Lawler, R.; Tang, W.; Bern, M.; Brodbelt, J. S. *J. Am. Soc. Mass Spectrom.* **2022**, *33* (3), 510−520.
(22) Smith, S. I.; Brodbelt, J. S. *Anal. Chem.* **2011**, *83* (1), 303−310.
(23) Madsen, J. A.; Brodbelt, J. S. *J. Am. Soc. Mass Spectrom.* **2010**, *21* (7), 1144−1150.
(24) Peters-Clarke, T. M.; Quan, Q.; Brademan, D. R.; Hebert, A. S.; Westphall, M. S.; Coon, J. J. *Anal. Chem.* **2020**, *92* (6), 4436−4444.
(25) Peters-Clarke, T. M.; Quan, Q.; Anderson, B. J.; McGee, W. M.; Lohr, E.; Hebert, A. S.; Westphall, M. S.; Coon, J. J. *Mol. Cell Proteomics* **2024**, *23* (4), 100742.
(26) Taucher, M.; Breuker, K. *Angew. Chem., Int. Ed.* **2012**, *51* (45), 11289−11292.
(27) Guzmán-Lorite, M.; Rosu, F.; Marina, M. L.; García, M. C.; Gabelica, V. *Anal. Chim. Acta* **2024**, *1299*, 342431.
(28) Largy, E.; König, A.; Ghosh, A.; Ghosh, D.; Benabou, S.; Rosu, F.; Gabelica, V. *Chem. Rev.* **2022**, *122* (8), 7720−7839.
(29) Anders, A. G.; Tidwell, E. D.; Gadkari, V. V.; Koutmos, M.; Ruotolo, B. T. *J. Am. Chem. Soc.* **2024**, *146* (7), 4412−4420.
(30) Heel, S. V.; Bartosik, K.; Juen, F.; Kreutz, C.; Micura, R.; Breuker, K. *J. Am. Chem. Soc.* **2023**, *145* (28), 15284−15294.
(31) Calderisi, G.; Glasner, H.; Breuker, K. *Angew. Chem., Int. Ed.* **2020**, *59* (11), 4309−4313.
(32) Goyon, A.; Nguyen, D.; Boulanouar, S.; Yehl, P.; Zhang, K. *Anal. Chem.* **2022**, *94* (48), 16960−16966.
(33) Goyon, A.; Scott, B.; Kurita, K.; Crittenden, C. M.; Shaw, D.; Lin, A.; Yehl, P.; Zhang, K. *Anal. Chem.* **2021**, *93* (44), 14792−14801.
(34) Goyon, A.; Scott, B.; Kurita, K.; Maschinot, C.; Meyer, K.; Yehl, P.; Zhang, K. *Anal. Chem.* **2022**, *94* (2), 1169−1177.
(35) Gau, B. C.; Dawdy, A. W.; Wang, H. L.; Bare, B.; Castaneda, C. H.; Friese, O. V.; Thompson, M. S.; Lerch, T. F.; Cirelli, D. J.; Rouse, J. C. *Sci. Rep.* **2023**, *13* (1), 9038.
(36) Wolf, E. J.; Grünberg, S.; Dai, N.; Chen, T. H.; Roy, B.; Yigit, E.; Corrêa, I. R. *Nucleic Acids Res.* **2022**, *50* (18), No. e106.
(37) Jiang, T.; Yu, N.; Kim, J.; Murgo, J. R.; Kissai, M.; Ravichandran, K.; Miracco, E. J.; Presnyak, V.; Hua, S. *Anal. Chem.* **2019**, *91* (13), 8500−8506.
(38) Hossain, M.; Limbach, P. A. *RNA* **2007**, *13* (2), 295−303.
(39) Vanhinsbergh, C. J.; Criscuolo, A.; Sutton, J. N.; Murphy, K.; Williamson, A. J. K.; Cook, K.; Dickman, M. J. *Anal. Chem.* **2022**, *94* (20), 7339−7349.
(40) Ross, R.; Cao, X.; Yu, N.; Limbach, P. A. *Methods* **2016**, *107*, 73−78.
(41) Yu, N.; Lobue, P. A.; Cao, X.; Limbach, P. A. *Anal. Chem.* **2017**, *89* (20), 10744−10752.
(42) Jora, M.; Borland, K.; Abernathy, S.; Zhao, R.; Kelley, M.; Kellner, S.; Addepalli, B.; Limbach, P. A. *Angew. Chem., Int. Ed.* **2021**, *60* (8), 3961−3966.
(43) Crittenden, C. M.; Lanzillotti, M. B.; Chen, B. *Anal. Chem.* **2023**, *95* (6), 3180−3186.
(44) Lanzillotti, M. B.; Brodbelt, J. S. *Anal. Chem.* **2024**, *96* (7), 3131−3136.
(45) Schneeberger, E.-M.; Breuker, K. *Angew. Chem., Int. Ed.* **2017**, *56* (5), 1254−1258.
(46) Schneeberger, E.-M.; Halper, M.; Palasser, M.; Heel, S. V.; Vušurović, J.; Plangger, R.; Juen, M.; Kreutz, C.; Breuker, K. *Nat. Commun.* **2020**, *11* (1), 5750.
(47) Kenderdine, T.; McIntyre, W.; Yassaghi, G.; Rollo, D.; Bunkowski, A.; Goerlach, L.; Suckau, D.; Tremintin, G.; Greig, M.; Bell, C.; et al. *J. Am. Soc. Mass Spectrom.* **2023**, *34* (10), 2296−2307.
(48) Huang, T. Y.; Liu, J.; McLuckey, S. A. *J. Am. Soc. Mass Spectrom.* **2010**, *21* (6), 890−898.
(49) Paul, D.; Marchand, A.; Verga, D.; Teulade-Fichou, M.-P.; Bombard, S.; Rosu, F.; Gabelica, V. *Analyst* **2019**, *144* (11), 3518−3524.
(50) Hannauer, F.; Black, R.; Ray, A. D.; Stulz, E.; Langley, G. J.; Holman, S. W. *Rapid Commun. Mass Spectrom.* **2023**, *37* (17), No. e9596.
(51) McLuckey, S. A.; Van Berkel, G. J.; Glish, G. L. *J. Am. Soc. Mass Spectrom.* **1992**, *3* (1), 60−70.
(52) Christofi, E.; Barran, P. *Chem. Rev.* **2023**, *123* (6), 2902−2949.
(53) Dodds, J. N.; Baker, E. S. *J. Am. Soc. Mass Spectrom.* **2019**, *30* (11), 2185−2195.
(54) Gabelica, V.; Marklund, E. *Curr. Opin. Chem. Biol.* **2018**, *42*, 51−59.
(55) Giles, K.; Ujma, J.; Wildgoose, J.; Pringle, S.; Richardson, K.; Langridge, D.; Green, M. *Anal. Chem.* **2019**, *91* (13), 8564−8573.
(56) Shaw, J. B.; Cooper-Shepherd, D. A.; Hewitt, D.; Wildgoose, J. L.; Beckman, J. S.; Langridge, J. I.; Voinov, V. G. *Anal. Chem.* **2022**, *94* (9), 3888−3896.
(57) Taucher, M.; Rieder, U.; Breuker, K. *J. Am. Soc. Mass Spectrom.* **2010**, *21* (2), 278−285.
(58) Sun, R.-X.; Zuo, M.-Q.; Zhang, J.-S.; Dong, M.-Q. *J. Am. Soc. Mass Spectrom.* **2023**, *34* (8), 1598−1608.

https://doi.org/10.1021/acs.analchem.5c00705
Anal. Chem. 2025, 97, 9430−9437

(59) Durbin, K. R.; Skinner, O. S.; Fellers, R. T.; Kelleher, N. L. *J. Am. Soc. Mass Spectrom.* **2015**, *26* (5), 782−787.
(60) Zenaidee, M. A.; Lantz, C.; Perkins, T.; Jung, W.; Loo, R. R. O.; Loo, J. A. *J. Am. Soc. Mass Spectrom.* **2020**, *31* (9), 1896−1902.
(61) Gao, Y.; McLuckey, S. A. *Journal of Mass Spectrometry* **2012**, *47* (3), 364−369.
(62) Meier, F.; Köhler, N. D.; Brunner, A.-D.; Wanka, J.-M. H.; Voytik, E.; Strauss, M. T.; Theis, F. J.; Mann, M. *Nat. Commun.* **2021**, *12* (1), 1185.

https://doi.org/10.1021/acs.analchem.5c00705
Anal. Chem. 2025, 97, 9430−9437